ACS APPLIED BIO MATERIALS

www.acsabm.org Article

Molybdenum Disulfide Supported on Metal−Organic Frameworks as an Ultrasensitive Layer for the Electrochemical Detection of the Ovarian Cancer Biomarker CA125

Shuang Li, Chang Hu, Chong Chen, Jiawei Zhang, Yongchang Bai, Cherie S. Tan, Guangjian Ni, Feng He,* Weifeng Li,* and Dong Ming*

Cite This: *ACS Appl. Bio Mater.* 2021, 4, 5494−5502 Read Online

ACCESS | Metrics & More | Article Recommendations | Supporting Information

ABSTRACT: Metal−organic frameworks (MOFs) are composed of metal ions/clusters and organic ligands, showing accessible functional sites, ultra-high porosity, and large specific surface area. Tricopper benzene-1,3,5-tricarboxylate (CuBTC), as a three-dimensional MOF architecture with an open and robust micro-/nanoconfiguration, possesses excellent catalytic performance and superior electric conductivity as compared to bulk MOF. In this study, CuBTC was used as a substrate on which molybdenum disulfide (MoS_2) was in situ constructed by a hydrothermal reaction to enhance the electron- and ion-transfer capability. Then, gold nanoparticles (AuNPs) were electroreduced on a CuBTC@MoS_2-modified electrode by linear sweep voltammetry for strengthening the connection between CA125 antibodies (CA125 Ab) and the substrate material. Due to the synergistic effect of CuBTC@MoS_2 and AuNPs, our biosensor showed excellent electrochemical performance. Subsequently, CuBTC@MoS_2-AuNPs/CA125 Ab-functionalized electrodes were used for the detection of the ovarian cancer biomarker CA125 from 0.5 mU/mL to 500 U/mL by differential pulse voltammetry. The results showed that the peak current decreased with the increase of concentration, and there was a logistic regression relationship between peak current variation and concentration. As interfering substances, carcinoembryonic antigen, human epididymis protein 4, and bovine serum albumin were applied for specific analysis. Our biosensor showed an obviously large response signal for CA125 detection than those observed for other interfering substances. Finally, serum samples collected from five patients were tested on our sensors with good consistency toward clinical standards, showing high practicability. This work demonstrated a tactic for simultaneously integrating the nanostructure, electroconductivity, and biocompatibility to construct advanced biosensors for cancer biomarkers.

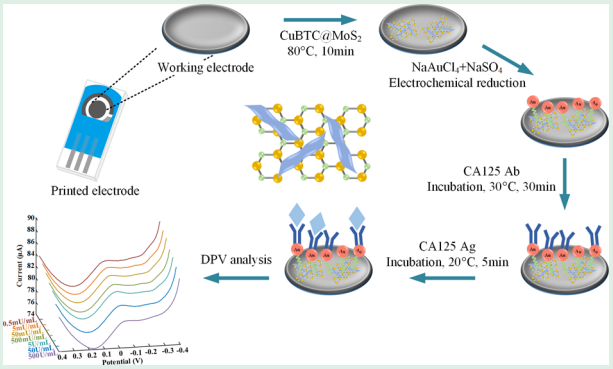

KEYWORDS: *metal−organic framework (MOF), tricopper benzene-1,3,5-tricarboxylate (CuBTC), molybdenum disulfide (MoS_2), CA125, ovarian cancer*

INTRODUCTION

Ovarian cancer is known to be a serious gynecological malignancy with a high mortality rate because of the insidious symptoms, high invasiveness, and propensity to metastasize. More than 70% patients with ovarian cancer were already in the advanced stage and cancer cells had spread beyond the pelvis at the time of treatment.[1] Therefore, there is an urgent clinical need for the early diagnosis of ovarian cancer as local stage disease can be cured effectively with a 5 yr survival rate of 93%.[2] Currently available diagnostic methods for cancer are as follows: pelvic ultrasound, computerized tomography, magnetic resonance imaging, and histopathological slices.[3,4] Nevertheless, imaging examination is expensive and a pathological section requires traumatic surgery due to which they are usually suitable for the examination of patients with advanced disease.

In contrast, detecting ovarian cancer biomarkers through body fluids is a more economical and convenient method for early screening.[5−8] According to research studies, cancer antigen 125 (CA125) is a commonly used marker to screen epithelial ovarian cancer and is the only approved marker for the subsequent cancer progression and treatment response.[9−11]

Received: March 16, 2021
Accepted: June 17, 2021
Published: June 29, 2021

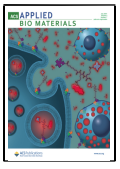

https://doi.org/10.1021/acsabm.1c00324
ACS Appl. Bio Mater. 2021, 4, 5494−5502

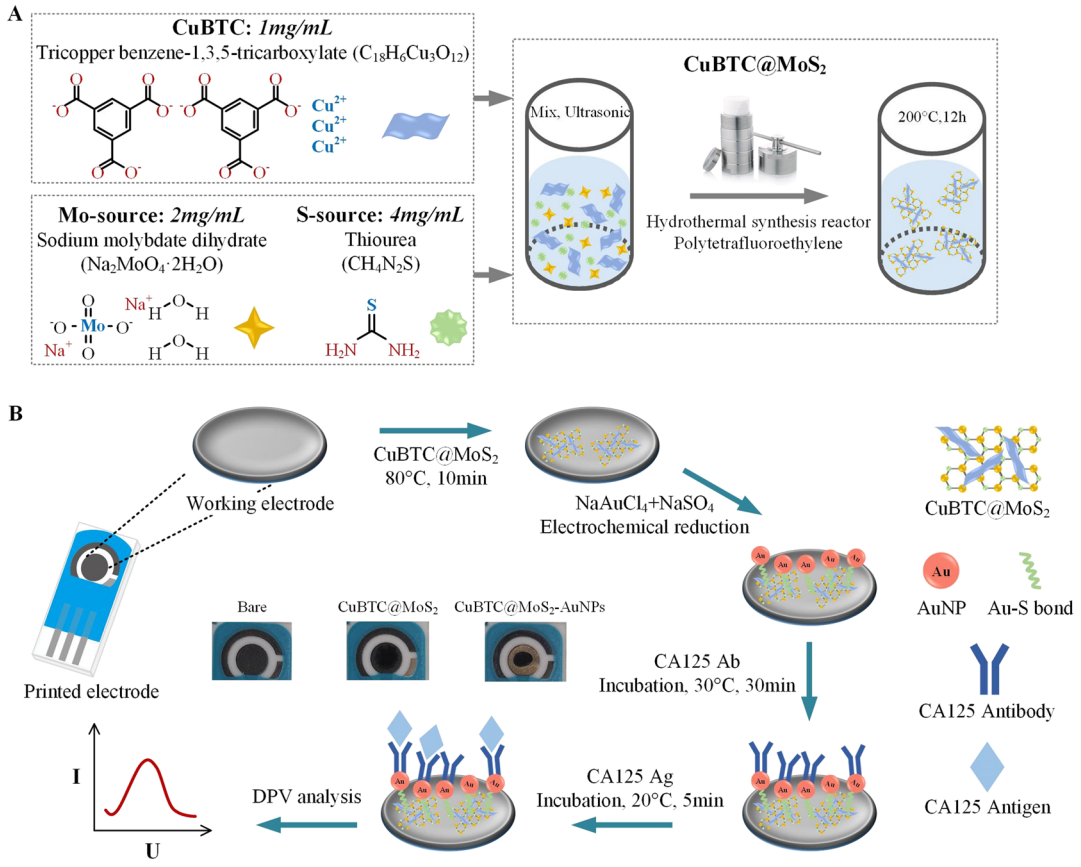

Figure 1. Schematic diagrams of the electrochemical sensing platform. (A) Synthesis of CuBTC@MoS_2. (B) Modification of printed electrodes with CuBTC@MoS_2-AuNPs for CA125 detection.

Therefore, there are increasing demands for the ultrasensitive detection of CA125 using rapid, reliable, and accurate techniques. Recently, enzyme-linked immunosorbent assays,[12] fluorescence spectrometry,[13] electrochemiluminescence,[14] electrochemistry,[15] surface plasmon resonance,[16] and luminescence resonance energy transfer[17] have been exploited for the quantitative detection of CA125. Among them, electrochemical immunosensors with high-affinity antibody−antigen binding are considered to be a promising strategy for fast response, low cost, high sensitivity, and selective detection. In order to reduce the detection limit and improve the signal to noise ratio of electrochemical biosensors, various advanced nanomaterials have been used to functionalize the biosensors.[18]

In particular, metal−organic frameworks (MOFs), as crystalline materials with a periodic network structure, have been considered to be a promising candidate due to their large surface area, high pore volume, and tailorable chemistry.[19−21] However, MOFs usually possessed disordered orientation and low conductivity, which were not conducive to electron transfer.[22] Research showed that MOFs could be used as precursors for metal sulfides and thus increase the conductivity and active sites as well as enhance the chemical adsorption capacity of polysulfide.[23,24] However, molybdenum disulfide (MoS_2) has an embeddable morphology, high electrochemical activity, and excellent chemical stability.[25] Wrapped MoS_2 is a polar substance and a catalyst, providing more active sites for nanocomposites.[26,27] Additionally, some electroactive MOFs such as Cu-based MOFs (tricopper benzene-1,3,5-tricarboxylate, CuBTC), possessing a three-dimensional (3D) porous honeycomb-like network, consist of blank metal sites to receive adsorbate molecules, which exhibit excellent catalytic performance and superior electric conductivity.[28] CuBTC is also thermostable and could be easily synthesized with relatively cheaper precursors compared to most of the MOFs.[29]

In this work, we proposed an ultrasensitive electrochemical biosensor by using the CuBTC@MoS_2 nanocomposites and gold nanoparticles (AuNPs) for the detection of the ovarian cancer biomarker CA125. Herein, CuBTC@MoS_2 nanocomposites were prepared by the hydrothermal method and modified on a printed electrode by thermal adsorption. Based on linear sweep voltammetry (LSV), AuNPs were prepared by reduction with sodium tetrachloroaurate on the CuBTC@MoS_2-modified electrode. Then, CA125 antibodies were immobilized onto the CuBTC@MoS_2-AuNP-functionalized electrode by electrostatic adsorption. Finally, the self-assembled electrodes were used for CA125 detection from 0.5 mU/mL to 500 U/mL by differential pulse voltammetry (DPV). To verify the specificity of our biosensor, carcinoembryonic antigen (CEA), human epididymis protein 4 (HE4), and bovine serum albumin (BSA) were analyzed. Furthermore, real patient serum samples were also tested for verifying the sensor accuracy. Here, the strategy of applying CuBTC@MoS_2-AuNPs as a sensing layer to achieve electrochemical analysis and enhance the sensitivity was reported for the first time. Moreover, the fabricated electrochemical immunosensors exhibited good performance in real-sample analysis, demonstrating its promising application in monitoring cancer biomarkers.

https://doi.org/10.1021/acsabm.1c00324
ACS Appl. Bio Mater. 2021, 4, 5494−5502

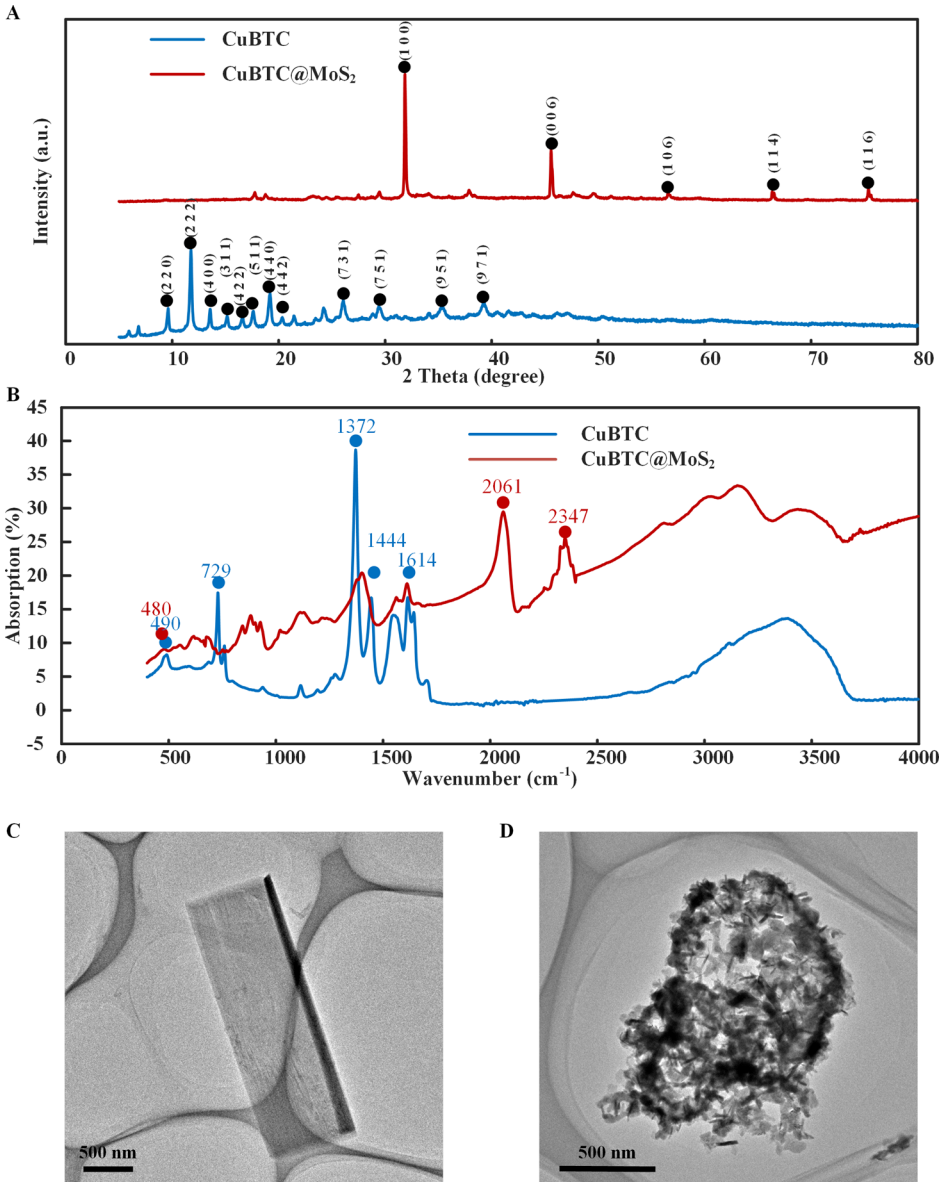

Figure 2. Characterization of nanocomposites. (A) XRD patterns of CuBTC and CuBTC@MoS_2. (B) ATR-FTIR absorbance spectra of CuBTC and CuBTC@MoS_2. (C) TEM images of CuBTC and (D) CuBTC@MoS_2.

EXPERIMENTAL SECTION

Chemicals and Materials. CuBTC was synthesized according to the mechanochemical method obtained from XFNANO (China). Chemicals for the synthesis of MoS_2 including sodium molybdate dihydrate ($Na_2MoO_4{\cdot}2H_2O$) and thiourea (CH_4N_2S); chemicals for the electrochemical reduction of AuNPs including sodium tetrachloroaurate(III) dihydrate ($NaAuCl_4{\cdot}2H_2O$) and sodium sulfate (Na_2SO_4); redox pairs used in electrochemical testing including potassium ferricyanide(III) ($K_3Fe(CN)_6$), potassium hexacyanoferrate(II) ($K_4Fe(CN)_6$), and potassium chloride (KCl) were all obtained from Sigma-Aldrich (USA). Phosphate buffered saline (PBS) (0.01 M, pH = 7.4), artificial serum, and BSA were obtained from Standard Information Network (China). The standard products of CA125 antigen (CA125 Ag), CA125 antibody (CA125 Ab), CEA, and HE4 were obtained from Roche (Switzerland). The printed electrodes used for electrochemical detection were obtained from Metrohm DropSens (Switzerland); the reference electrode was Ag/AgCl and the working and counter electrodes were carbon.

CuBTC@MoS_2 Synthesis. CuBTC (1 mg/mL), $Na_2MoO_4{\cdot}2H_2O$ (2 mg/mL), and CH_4N_2S (4 mg/mL) were mixed and ultrasonicated to obtain a homogeneous solution. Then, the mixed solution was transferred into a Teflon-lined autoclave and reacted at 200 °C for 12 h (Figure 1A). CuBTC@MoS_2 was collected by centrifugation and dried at 80 °C. Finally, 1 mg/mL CuBTC@MoS_2 was re-dispersed in water for further experiments. Qualitative identification of the phase composition and structure was done by X-ray diffraction (XRD) on a MiniFlex600 (Japan). Chemical bonds of CuBTC@MoS_2 were measured by attenuated total reflection Fourier transform infrared spectroscopy (ATR-FTIR) on a Bruker TENSOR II (Germany). A Tecnai G2 F20 (The Netherlands) transmission electron microscope with 200 kV accelerating voltage was used for the morphological characterization of CuBTC@MoS_2. Scanning electron microscopy (SEM) was carried out on a NanoSEM 430 (United States) to show the micromorphology of the CuBTC@MoS_2 powder. A particle size analyzer (Litesizer 500, Anton Paar Co., Austria) was used to determine the CuBTC@MoS_2 particle size distribution.

Biosensor Modification. Before modification, electrodes were washed by water and ethanol. Next, 4 μL of CuBTC@MoS_2 was dropped on the carbon working electrode, whose shape was a circle with a diameter of 4 mm. Then, it was placed in an oven at 80 °C for 10 min, after which a CuBTC@MoS_2 sensitive layer was formed (Figure 1B). For electrodeposition of AuNPs, 1% $NaAuCl_4$ and 0.5 M

https://doi.org/10.1021/acsabm.1c00324
ACS Appl. Bio Mater. 2021, 4, 5494−5502

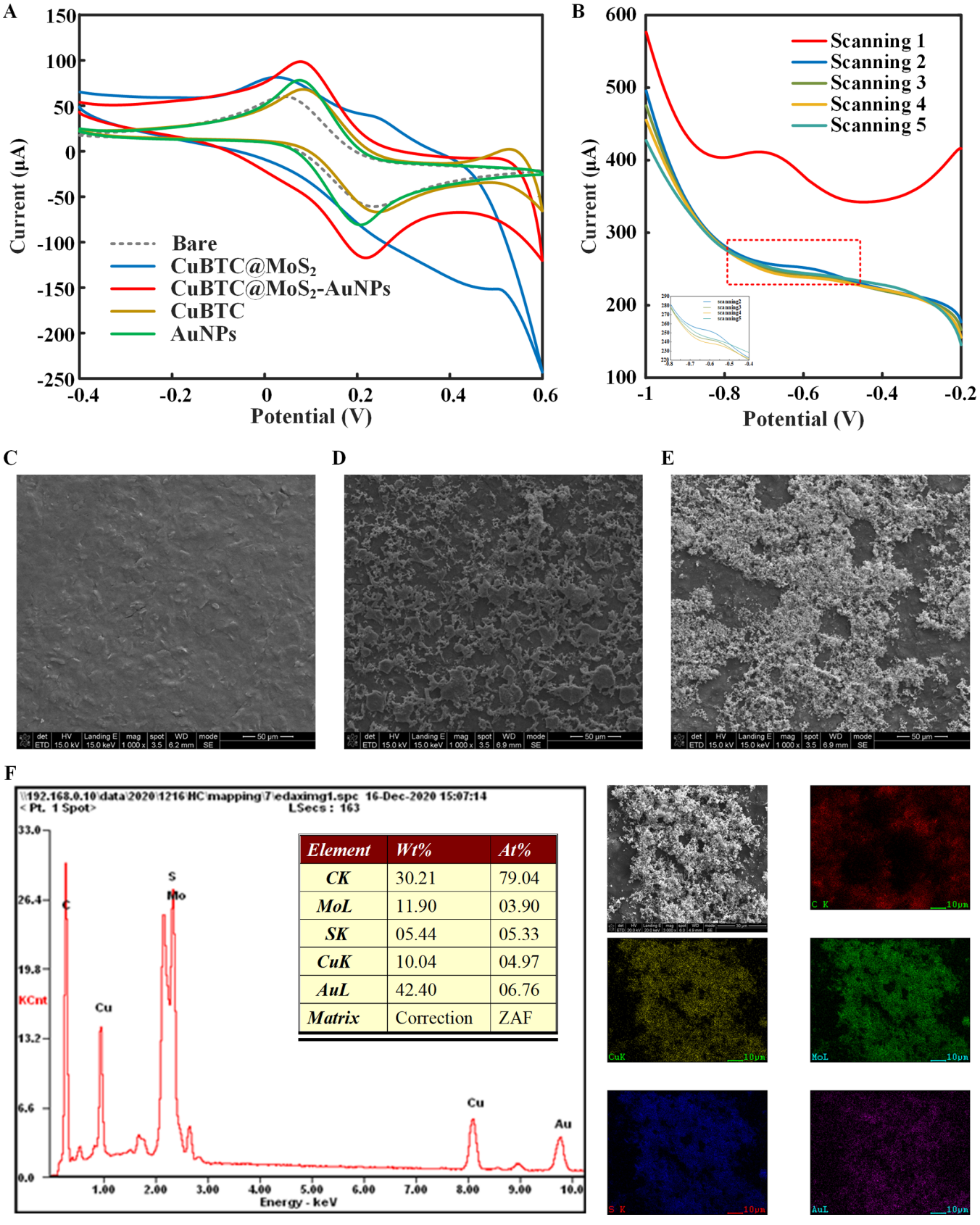

Figure 3. Characterization of electrodes. (A) CV curves of the bare, CuBTC@MoS_2, CuBTC@MoS_2-AuNP, CuBTC, and AuNP electrodes obtained in the redox pair containing $[Fe(CN)_6]^{3-/4-}$ (5 mM) and KCl (0.5 M). (B) LSV scanning for the electrochemical reduction of AuNPs in the electrolyte containing $NaAuCl_4$ (1%) and $NaSO_4$ (0.5 M). (C) SEM images of the bare electrode, (D) CuBTC@MoS_2-modified electrode, and (E) CuBTC@MoS_2-AuNP-modified electrode. (F) EDS spectrum of the CuBTC@MoS_2-AuNP-modified electrode.

https://doi.org/10.1021/acsabm.1c00324
ACS Appl. Bio Mater. 2021, 4, 5494−5502

$NaSO_4$ of equal volumes were mixed as the electrolyte. LSV scanning from −0.2 to −1.0 V with a 0.1 V/s scan rate was performed on the electrode to modify the AuNPs. Finally, the specific antibody CA125 Ab (0.1 mg/mL) was incubated at 30 °C for 30 min on CuBTC@MoS_2-AuNP-functionalized electrodes. The modified electrodes were washed with PBS for removing unbound CA125 Ab. Electrochemical characterization of the electrode was performed by cyclic voltammetry (CV) from −0.4 to 0.6 V with a 0.05 V/s scan rate. Here, LSV and CV scans were all carried on a CHI660E (China) electrochemical workstation. SEM was used to show the micromorphology of the electrode surface. Energy-dispersive X-ray spectroscopy (EDS) was carried out and EMSA/MAS (United Kingdom) was used for elemental analysis.

CA125 Detection. DPV was employed to detect CA125 from 0.5 mU/mL to 500 U/mL on CHI660E (China). Here, the sweep voltage range was −0.4 to 0.4 V; the amplitude voltage was 0.05 V; and the pulse width was 0.05 s. Furthermore, CEA (5 ng/mL), HE4 (140 pM), and BSA (10 ng/mL) with the cut-off value of clinical examination were detected by DPV for specific analysis with the same parameters as CA125 detection. Finally, five patient serum samples from Tianjin Medical University Cancer Institute and Hospital with the gold standard CA125 test results of 73.1 U/mL (Sample 1), 9.06 U/mL (Sample 2), 109 U/mL (Sample 3), 594 U/mL (Sample 4), and 36.3 U/mL (Sample 5) were tested for verifying the accuracy of our CA125 biosensor.

RESULTS AND DISCUSSION

CuBTC@MoS_2 Features. The XRD patterns of nanomaterials are shown in Figure 2A. A scan rate of 0.02°/s was used to record the spectra from 5 to 80°. The peaks were clear and sharp, which indicated that CuBTC and CuBTC@MoS_2 samples had good crystallinity. Twelve major peaks found at 9.60, 11.76, 13.56, 14.70, 16.60, 17.60, 19.18, 20.34, 26.06, 29.40, 35.40, and 39.22° corresponded to the (220), (222), (400), (311), (422), (511), (440), (442), (731), (751), (951), and (971) crystal planes, respectively. After the growth of the MoS_2 layer, the peaks with 2 theta of 31.88, 45.62, 56.62, 66.42, and 75.42° were observed, which corresponded to (100), (006), (106), (114), and (116) of 2H−MoS_2 (JCPDS 37-1492), respectively. A significant increase of the peak at (100) revealed that MoS_2 mostly grew along the −COOH functional group of CuBTC. The growth of MoS_2 sheets will compete with Cu ions for the −COOH functional group, which ultimately influences the growth direction of the crystal.

Figure 2B shows the ATR-FTIR spectral results of CuBTC and CuBTC@MoS_2 from 400 to 4000 cm^{-1}. The Cu−O vibration of CuBTC was observed at 490 cm^{-1}. Vibrations of C−H out-of-plane bending were reflected at 729 cm^{-1}, indicating the presence of aromatic structures. Peaks at 1372 and 1444 cm^{-1} represent the C═O bonds of carboxylic groups. The peak at 1614 cm^{-1} represents the C═O stretching of CuBTC. In the range of 1900 to 2500 cm^{-1}, there were absorption bands produced by the stretching vibration of a triple bond or cumulative double bond. At high temperatures and pressures, two kinds of derivatives were formed. The source of Mo and CuBTC were connected in the form of C═O═C (2347 cm^{-1}), and the source of S and CuBTC were connected in the form of −C═C−N (2061 cm^{-1}). It is reported that the infrared peak of MoS_2 was observed around 460 cm^{-1}.[30,31] As the previous XRD results indicate, MoS_2 grew along the −COOH functional group, which may hinder the peak from the Cu−O bond at 490 cm^{-1}. Therefore, the Mo−S vibration resulted in a peak at 480 cm^{-1} in the ATR-FTIR spectrum of CuBTC@MoS_2. The XRD and ATR-FTIR results illustrate the phase composition and functional groups of CuBTC@MoS_2, which also prove the successful synthesis.

TEM results of CuBTC and CuBTC@MoS_2 show the micromorphology of nanomaterials. As shown in Figure 2C, the shape of CuBTC was prismatic with the size of a micron scale. Figure S1 shows the SEM and particle size distribution results of CuBTC powder, whose particle size was concentrated at about 2 μm. After loading MoS_2, CuBTC@MoS_2 showed more wrinkle morphology and a smaller size than CuBTC (Figure 2D). The SEM result of CuBTC@MoS_2 clearly shows the layered stack, where CuBTC was wrapped (Figure S2). Besides, the particle size distribution of CuBTC@MoS_2 was mainly 200 nm. However, another peak was observed at 1500 nm, which might be due to the stacking of lamellae (Figure S2). All these results reveal the synthesis of CuBTC@MoS_2 and its micromorphology for subsequent applications.

Electrode Characterization. Figure 3A demonstrates the electrochemical characterization of the bare, CuBTC@MoS_2, and CuBTC@MoS_2-AuNP-modified electrodes. As control groups, CV results of the electrodes modified only with CuBTC and only with AuNPs are also shown in Figure 3A. Here, 70 μL of 5 mM $[Fe(CN)_6]^{3-/4-}$ containing 0.5 M KCl was added on electrodes as a redox pair. CV scanning from −0.4 to 0.6 V (vs Ag/AgCl) was performed for the above electrodes. The results show that the peaks of the reduction current of the bare electrode, CuBTC@MoS_2-modified electrode, and CuBTC@MoS_2-AuNP-modified electrode were 60.27, 81.4, and 98.59 μA, respectively. With the modification of nanocomposites, electrochemical characteristics of the electrode gradually enhanced. When the electrode was only CuBTC-modified the reduction current increased to 68.14 μA, the reduction voltage also increased from 0.042 to 0.083 V, which may increase the electrochemical reaction difficulty. This may be due to the potential pseudocapacitive sites in CuBTC. When CuBTC@MoS_2 modified an electrode, the reduction current increased to 81.4 μA with the voltage decreasing to 0.025 V. Therefore, CuBTC@MoS_2 greatly improved the electrochemical performance of the electrode. MoS_2 with strong van der Waals interactions present in lamellar crystals and shortened electron-/ion-transfer distance served as an electroactive material that improved the electrical conductivity.[32]

Then, AuNPs with excellent biocompatibility and stable electrochemical characteristics were modified as the top layer of the self-assembled electrode. Figure 3B shows the electrochemical reduction and deposition processes, during which the peak of the reduction voltage was −0.714 V at the first scanning, and the next scanning mainly realized the deposition process. With the modification of AuNPs, the current signal was further amplified from 81.4 to 98.59 μA compared to the CuBTC@MoS_2 electrode. Moreover, if only AuNPs were deposited on an electrode, the reduction current was only 78.16 μA, which was far less than that of the designed CuBTC@MoS_2-AuNP electrode. With the modification of CA125 antibodies, the peak current decreased in the CV curve (Figure S3).

SEM images are shown in Figure 3C−E, which indicate the dispersion and distribution of the nanocomposites on an electrode. With the self-assembly functionalization, more active edges and surfaces have been created. Figure S4 shows the local magnification result of the CuBTC@MoS_2-modified electrode, in which clear columnar and lamellar morphologies

https://doi.org/10.1021/acsabm.1c00324
ACS Appl. Bio Mater. 2021, 4, 5494−5502

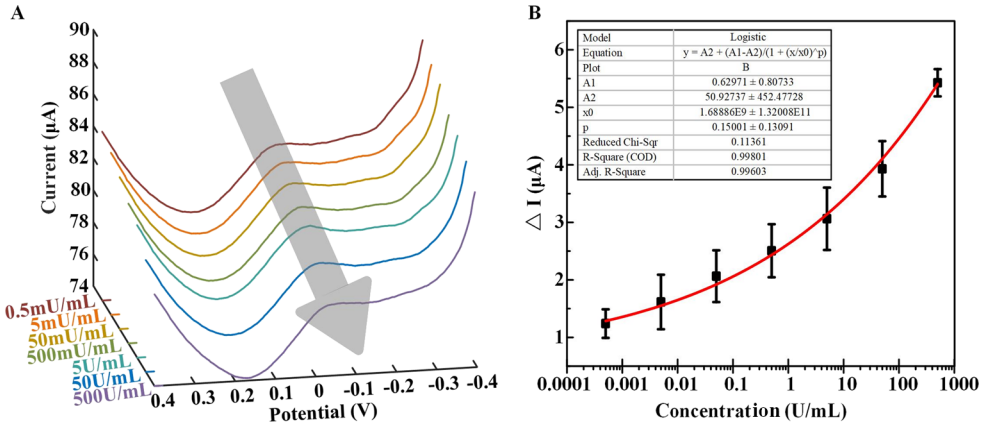

Figure 4. CA125 detection. (A) DPV 3D-curves of CA125 detection from 0.0005 to 500 U/mL in PBS (0.01 M, pH = 7.4). (B) Logistic regression fitting curve between the concentration and the current difference ($\Delta I = I_{PBS} - I_{CA125}$).

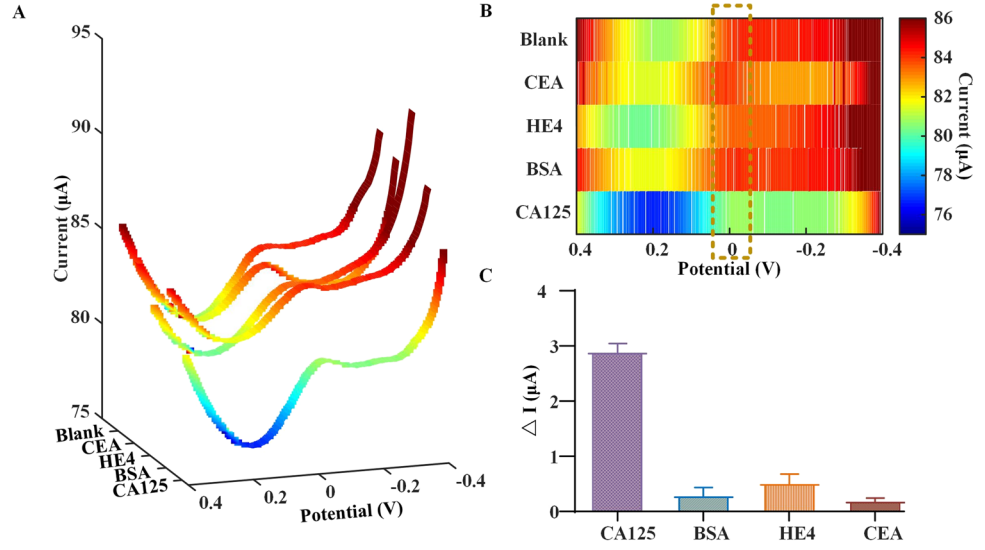

Figure 5. Specificity analysis. (A) 3D heat maps, (B) 2D heat maps, and (C) column charts of CA125 (35 U/mL), BSA (10 ng/mL), HE4 (140 pM), and CEA (5 ng/mL) detection.

were identified. However, AuNPs can be seen in Figure S5. In addition to observing the self-assembly process of the electrode morphologically, EDS analysis was used to illustrate the elemental distribution on the electrode. Figure S6 shows the EDS spectrum of the substrate carbon electrode, in which the C element was evenly distributed on the electrode surface. Figure S7 shows the EDS result of the CuBTC@MoS_2-modified electrode, in which Cu, Mo, and S elements covered the electrode surface. The EDS result of the CuBTC@MoS_2-AuNP electrode is shown in Figure 3F, in which Cu, Mo, S, and Au were located in the same area. These results elucidated the related characteristics of the electrode modified with nanocomposites, from the perspectives of electrochemical analysis and micromorphological distribution, and provided technical support for subsequent biosensing.

CA125 Biosensing. Before CA125 biosensing, CA125 antibodies were modified on the electrode as a specific recognition layer. DPV analysis of CA125 from 0.5 mU/mL to 500 U/mL is shown in Figure 4A. Here, the voltage is taken in the *X*-axis, current in the *Y*-axis, and concentration in the *Z*-axis, forming a 3D distribution map. Figure S8 shows the 2D DPV results, in which as the concentration of CA125 increased, the peak current decreased gradually from 83.1 to 78.4 μA. Next, a plot is constructed with the current difference ($\Delta I = I_{PBS} - I_{CA125}$) as the vertical axis and the logarithmic distribution of concentration as the horizontal axis. Frequently, logistic regression analysis, as a generalized linear regression analysis model, was used in data mining, automatic disease diagnosis, and economic forecasting. Logistic regression was used to find that Δ*I* had a good correlation with the CA125 concentration, in which the correlation coefficient was as high as 0.99801 (Figure 4B).

To analyze the selectivity of the proposed strategy, the electrochemical immunosensor was applied to detect possible interferents with their thresholds, such as BSA (10 ng/mL), CEA (5 ng/mL), and HE4 (140 pM). The 3D heat maps in Figure 5A show the electrochemical response curves; the higher the peak current, the redder the color. Figure S9 shows the plane result of DPV analysis with the peak voltage distributed from −0.05 to 0.05 V. The peak currents of CEA, HE4, and BSA are around 84 μA, close to those of the control group; only the peak current of CA125 declined to 81 μA. Figure 5B shows the 2D heat maps, in which the peak current of CA125 (35 U/mL) was obviously low. The color of the peak current (green) during CA125 detection was obviously lighter than that of other interfering substances (red) in the

https://doi.org/10.1021/acsabm.1c00324
ACS Appl. Bio Mater. 2021, 4, 5494−5502

Table 1. Comparison of Our Sensor with Other Electrochemical Immunosensors for CA125 Detection[a]

type	materials	method	range (U/mL)	LOD (U/mL)	references
i−*t*	CS-AuNP/MWCNT/GO	CA	0.01−100	0.002	33
Z−*f*	MPA/AuNP@SiO_2/QD	EIS	0−0.1	0.0016	34
l−*u*	Fe_3O_4@g-C_3N_4	ECL	0.001−5	0.0004	35
i−*u*	3DrGO-MWCNT-PAMAM/AuNPs	SWV	0.0005−75	6 μL	36
	ZnO nanorods−AuNPs	CV	2.5−1000 ng/μL	2.5 ng/μL	37
	poly(anthranilic acid)	ASV	5−25	2	38
	CuBTC@MoS_2-AuNPs	DPV	0.0005−500	0.0005	present work

[a]LOD: limit of detection; 3DrGO-MWCNTs: three-dimensional reduced graphene oxide-multiwalled carbon nanotubes; PAMAM: polyamidoamine; AgNPs-PAN-oxime NFs: silver nanoparticle-doped amidoxime-modified polyacrylonitrile nanofibers; CS-AuNP/MWCNT/GO: chitosan-gold nanoparticle/multiwalled carbon nanotube/graphene oxide; CA: chronoamperometry; g-C3N4: graphitic carbon nitride; ECL: electrochemiluminescence; MPA: mercaptopropionic acid; QD: CdSe quantum dots; EIS: electrochemical impedance spectroscopy; ASV: anodic stripping voltammetry.

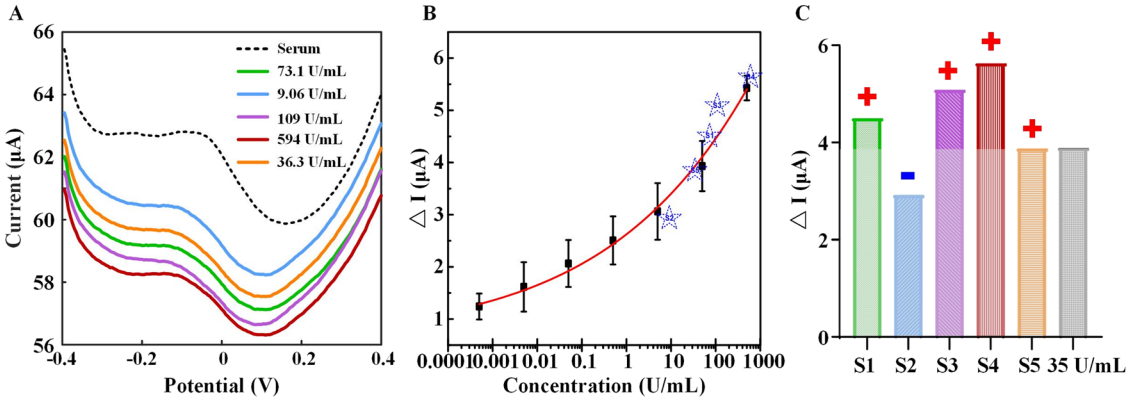

Figure 6. Clinical sample testing. (A) DPV detection of serum samples with CA125 gold standard test results of 73.1, 9.06, 109, 594, and 36.3 U/mL. (B) Relative positions of five samples on the concentration fitting curve. (C) Qualitative analysis of the samples.

heat map, which means our electrode can detect CA125 specifically without the interference of HE4, BSA, and CEA. Statistical histograms reflected that the change in the peak current during CA125 detection was significantly higher than that of other groups (Figure 5C). All these results indicated that our sensor had a wide detection range from 0.5 mU/mL to 500 U/mL, a low detection limit of 0.5 mU/mL, and excellent specificity for CA125 detection.

Table 1 shows different kinds of electrochemical methods combined with sensitive materials for CA125 detection. It can be roughly divided into four categories: current−time (*i*−*t*), impedance−frequency (*Z*−*f*), luminescence−voltage (*l*−*u*), and current−voltage (*i*−*u*). Relatively speaking, the electrochemical technology of the current−voltage type showed a wider detection range and a lower detection limit. In this study, CuBTC@MoS_2-AuNPs played a critical role in the electrochemical signal amplification and provided a novel sensing platform for DPV analysis. A 3D structure coupled with high stability and porosity made CuBTC an excellent platform for increasing the electrochemical reaction sites and growing the MoS_2 lamella, which served as a kind of substrate to enhance the electron-transfer capability. Composites of CuBTC@MoS_2 provided more binding sites for AuNPs, which further increased the conductivity and could immobilize a large number of specific antibodies. Therefore, we can say that our CuBTC@MoS_2-AuNPs/CA125 Ab-based immunosensor possessed good performance in CA125 detection, laying a solid foundation for clinical applications.

Clinical Sample Testing. Tianjin Medical University Cancer Institute and Hospital provided serum samples of five patients, whose gold standard test results of CA125 concentration were 73.1, 9.06, 109, 594, and 36.3 U/mL. Figure 6A shows the DPV analysis of these samples, in which the peak current decreased with the increase of CA125 concentration. Here, $\Delta I = I_{serum} - I_{sample}$, where I_{serum} is the peak current of DPV only in the artificial serum and I_{sample} is the peak current of DPV in the serum samples from five patients. Figure 6B shows the relative positions of the five samples in the concentration fitting curve. In Figure 6C, the current value corresponding to the cut-off value of 35 U/mL was used for the qualitative analysis of samples, and the finding was found to be consistent with the clinical test result. It showed that our immunosensor can be considered as a promising platform for the detection of CA125 and the evaluation of negative and positive in ovarian cancer with acceptable accuracy and reliability.

CONCLUSIONS

In this study, CuBTC composited with MoS_2 was proposed as a sensing material for the ultrasensitive detection of biomarkers for the first time. CuBTC@MoS_2 was synthesized by the hydrothermal method showing excellent electrochemical performance with rapid electron- and ion-transfer capability, which were predominantly ascribed to the strong confinement effect. Furthermore, AuNPs were loaded onto CuBTC@MoS_2 for strengthening the connection between the substrate material and biomolecules. Along these lines, the presence of highly functional groups played a critical role in the covalent modification of the sensing layer and the signal layer. Due to the synergistic effect of AuNPs and CuBTC@MoS_2, our

https://doi.org/10.1021/acsabm.1c00324
ACS Appl. Bio Mater. 2021, 4, 5494−5502

biosensor showed excellent electrochemical performance. Finally, the CuBTC@MoS_2-AuNPs/CA125 Ab-modified electrodes were applied for CA125 sensing from 0.5 mU/mL to 500 U/mL with the LOD of 0.5 mU/mL. Even in the presence of BSA, HE4, and CEA interfering substances, our sensor displayed excellent specificity for CA125. In view of this, real patient serum samples were also tested by our platform, showing good consistency toward the clinical standard. This demonstrated the promising application of the fabricated electrochemical immunosensors in monitoring cancer biomarkers.

■ ASSOCIATED CONTENT

Supporting Information

The Supporting Information is available free of charge at https://pubs.acs.org/doi/10.1021/acsabm.1c00324.

Morphology characterization of CuBTC and CuBTC@MoS_2, CV characterization of CA125 antibody-modified electrode, morphology characterization and EDS analysis of electrodes, and DPV curves of CA125 detection (PDF)

■ AUTHOR INFORMATION

Corresponding Authors

Feng He − *Academy of Medical Engineering and Translational Medicine and Department of Biomedical Engineering, College of Precision Instruments and Optoelectronics Engineering, Tianjin University, Tianjin 300072, China*; Email: heaven@tju.edu.cn

Weifeng Li − *Academy of Medical Engineering and Translational Medicine, Tianjin University, Tianjin 300072, China; Tianjin International Engineering Institute, Tianjin University, Tianjin 300072, China*; Email: bsh@tju.edu.cn

Dong Ming − *Academy of Medical Engineering and Translational Medicine and Department of Biomedical Engineering, College of Precision Instruments and Optoelectronics Engineering, Tianjin University, Tianjin 300072, China*; Phone: +86 022-83612122; Email: richardming@tju.edu.cn; Fax: +86 022-83612122

Authors

Shuang Li − *Academy of Medical Engineering and Translational Medicine, Tianjin University, Tianjin 300072, China*; orcid.org/0000-0002-3483-5087

Chang Hu − *Academy of Medical Engineering and Translational Medicine, Tianjin University, Tianjin 300072, China; Tianjin International Engineering Institute, Tianjin University, Tianjin 300072, China*

Chong Chen − *Academy of Medical Engineering and Translational Medicine, Tianjin University, Tianjin 300072, China; Department of Clinical Laboratory, Tianjin Medical University Cancer Institute and Hospital, Tianjin 300060, China*

Jiawei Zhang − *Academy of Medical Engineering and Translational Medicine, Tianjin University, Tianjin 300072, China*

Yongchang Bai − *Academy of Medical Engineering and Translational Medicine, Tianjin University, Tianjin 300072, China*

Cherie S. Tan − *Academy of Medical Engineering and Translational Medicine, Tianjin University, Tianjin 300072, China*; orcid.org/0000-0003-1612-6241

Guangjian Ni − *Academy of Medical Engineering and Translational Medicine and Department of Biomedical Engineering, College of Precision Instruments and Optoelectronics Engineering, Tianjin University, Tianjin 300072, China*

Complete contact information is available at: https://pubs.acs.org/10.1021/acsabm.1c00324

Notes

The authors declare no competing financial interest.

■ ACKNOWLEDGMENTS

This work was supported by the National Natural Science Foundation of China (award no: 82001922), Postdoctoral Research Foundation of China (award no: 2019M661025 and 2020T130467), Tianjin S&T Major Project of Artificial Intelligence (award no: 17ZXRGGX00020), Tianjin Natural Science Foundation (award no: 20JCQNJC01800), and Tianjin S&T Development Fund of Education Commission for Higher Education (award no: 2018KJ048).

■ REFERENCES

(1) Franier, B. D. L.; Thompson, M. Early stage detection and screening of ovarian cancer: A research opportunity and significant challenge for biosensor technology. *Biosens. Bioelectron.* **2019**, *135*, 71−81.

(2) Siegel, R. L.; Miller, K. D.; Jemal, A. Cancer statistics, 2020. *Ca-Cancer J. Clin.* **2020**, *70*, 7−30.

(3) Sharma, S.; Raghav, R.; O'Kennedy, R.; Srivastava, S. Advances in ovarian cancer diagnosis: A journey from immunoassays to immunosensors. *Enzyme Microb. Technol.* **2016**, *89*, 15−30.

(4) Valentini, A. L.; Gui, B.; Micco, M.; Mingote, C.; De Gaetano, M.; Ninivaggi, V.; Bonomo, L. Benign and Suspicious Ovarian Masses-MR Imaging Criteria for Characterization: Pictorial Review. *J. Oncol.* **2012**, *2012*, 481806.

(5) Hulstaert, E.; Morlion, A.; Levanon, K.; Vandesompele, J.; Mestdagh, P. Candidate RNA biomarkers in biofluids for early diagnosis of ovarian cancer: A systematic review. *Gynecol. Oncol.* **2021**, *160*, 633−642.

(6) Shabaninejad, Z.; Vafadar, A.; Movahedpour, A.; Ghasemi, Y.; Namdar, A.; Fathizadeh, H.; Pourhanifeh, M. H.; Savardashtaki, A.; Mirzaei, H. Circular RNAs in cancer: new insights into functions and implications in ovarian cancer. *J. Ovarian Res.* **2019**, *12*, 84−96.

(7) Guo, C.; Song, C.; Zhang, J.; Gao, Y.; Qi, Y.; Zhao, Z.; Yuan, C. Revisiting Chemoresistance in Ovarian Cancer: Mechanism, biomarkers, and precision medicine. *Genes Dis.* **2020**. In Press. https://doi.org/10.1016/j.gendis.2020.11.017.

(8) Muinao, T.; Boruah, D.; Pal, M. Multi-biomarker panel signature as the key to diagnosis of ovarian cancer. *Heliyon* **2019**, *5*, No. e02826.

(9) Szymanska, B.; Lukaszewski, Z.; Hermanowicz-Szamatowicz, K.; Gorodkiewicz, E. An immunosensor for the determination of carcinoembryonic antigen by Surface Plasmon Resonance Imaging. *Anal. Biochem.* **2020**, *609*, 113964.

(10) Saadati, A.; Hassanpour, S.; Bahavarnia, F.; Hasanzadeh, M. A novel biosensor for the monitoring of ovarian cancer tumor protein CA 125 in untreated human plasma samples using a novel nano-ink: a new platform for efficient diagnosis of cancer using paper based microfluidic technology. *Anal. Methods* **2020**, *12*, 1639−1649.

(11) Zhang, M.; Cheng, S.; Jin, Y.; Zhao, Y.; Wang, Y. Roles of CA125 in diagnosis, prediction, and oncogenesis of ovarian cancer. *Biochim. Biophys. Acta Rev. Canc* **2021**, *1875*, 188503.

(12) Alberti, D.; van't Erve, M.; Stefania, R.; Ruggiero, M. R.; Tapparo, M.; Crich, S.; Aime, S. A Quantitative Relaxometric Version of the ELISA Test for the Measurement of Cell Surface Biomarkers. *Angew. Chem. Int. Ed.* **2014**, *53*, 3488−3491.

(13) Chen, F.; Liu, Y.; Chen, C.; Gong, H.; Cai, C.; Chen, X. Respective and simultaneous detection tumor markers CA125 and STIP1 using aptamer-based fluorescent and RLS sensors. *Sens. Actuators, B* **2017**, *245*, 470−476.
(14) Babamiri, B.; Hallaj, R.; Salimi, A. Ultrasensitive electrochemiluminescence immunoassay for simultaneous determination of CA125 and CA15-3 tumor markers based on PAMAM-sulfanilic acid-Ru(bpy)(3)(2+) and PAMAM-CdTe@CdS nanocomposite. *Biosens. Bioelectron.* **2018**, *99*, 353−360.
(15) de Castro, A. C. H.; Alves, M.; Silva, C.; Madurro, M.; Brito, G. Label-free electrochemical immunosensor for detection of oncomarker CA125 in serum. *Microchem. J.* **2020**, *155*, 104746.
(16) Szymańska, B.; Lukaszewski, Z.; Hermanowicz, K.; Gorodkiewicz, E. A biosensor for determination of the circulating biomarker CA125/MUC16 by Surface Plasmon Resonance Imaging. *Talanta* **2020**, *206*, 120187.
(17) Zhang, X.; Wang, Y.; Deng, H.; Xiong, X.; Zhang, H.; Liang, T.; Li, C. An aptamer biosensor for CA125 quantification in human serum based on upconversion luminescence resonance energy transfer. *Microchem. J.* **2021**, *161*, 105761.
(18) Sharifi, M.; Avadi, M. R.; Attar, F.; Dashtestani, F.; Ghorchian, H.; Rezayat, S. M.; Saboury, A. A.; Falahati, M. Cancer diagnosis using nanomaterials based electrochemical nanobiosensors. *Biosens. Bioelectron.* **2019**, *126*, 773−784.
(19) Bieniek, A.; Terzyk, A. P.; Wiśniewski, M.; Roszek, K.; Kowalczyk, P.; Sarkisov, L.; Keskin, S.; Kaneko, K. MOF materials as therapeutic agents, drug carriers, imaging agents and biosensors in cancer biomedicine: Recent advances and perspectives. *Prog. Mater. Sci.* **2021**, *117*, 100743.
(20) Li, X.; Li, X.; Li, D.; Zhao, M.; Wu, H.; Shen, B.; Liu, P.; Ding, S. Electrochemical biosensor for ultrasensitive exosomal miRNA analysis by cascade primer exchange reaction and MOF@Pt@MOF nanozyme. *Biosens. Bioelectron.* **2020**, *168*, 112554.
(21) Chang, J.; Wang, X.; Wang, J.; Li, H.; Li, F. Nucleic Acid-Functionalized Metal-Organic Framework-Based Homogeneous Electrochemical Biosensor for Simultaneous Detection of Multiple Tumor Biomarkers. *Anal. Chem.* **2019**, *91*, 3604−3610.
(22) Deng, T.; Lu, Y.; Zhang, W.; Sui, M.; Shi, X.; Wang, D.; Zheng, W. Inverted Design for High-Performance Supercapacitor Via Co(OH)(2)-Derived Highly Oriented MOF Electrodes. *Adv. Energy Mater.* **2018**, *8*, 1702294.
(23) Fang, D.; Wang, Y.; Qian, C.; Liu, X.; Wang, X.; Chen, S.; Zhang, S. Synergistic Regulation of Polysulfides Conversion and Deposition by MOF-Derived Hierarchically Ordered Carbonaceous Composite for High-Energy Lithium-Sulfur Batteries. *Adv. Funct. Mater.* **2019**, *29*, 1900875.
(24) Chen, K.; Sun, Z.; Fang, R.; Shi, Y.; Cheng, H.-M.; Li, F. Metal-Organic Frameworks (MOFs)-Derived Nitrogen-Doped Porous Carbon Anchored on Graphene with Multifunctional Effects for Lithium-Sulfur Batteries. *Adv. Funct. Mater.* **2018**, *28*, 1707592.
(25) Anichini, C.; Czepa, W.; Pakulski, D.; Aliprandi, A.; Ciesielski, A.; Samorì, P. Chemical sensing with 2D materials. *Chem. Soc. Rev.* **2018**, *47*, 4860−4908.
(26) Sun, C.; Zhao, K.; He, Y.; Zheng, J.; Xu, W.; Zhang, C.; Wang, X.; Guo, M.; Mai, L.; Wang, C.; Gu, M. Interconnected Vertically Stacked 2D-MoS2 for Ultrastable Cycling of Rechargeable Li-Ion Battery. *ACS Appl. Mater. Interfaces* **2019**, *11*, 20762−20769.
(27) Muthurasu, A.; Maruthapandian, V.; Kim, H. Y. Metal-organic framework derived Co3O4/MoS2 heterostructure for efficient bifunctional electrocatalysts for oxygen evolution reaction and hydrogen evolution reaction. *Appl. Catal., B* **2019**, *248*, 202−210.
(28) Cao, Y.; Wang, L.; Shen, C.; Wang, C.; Hu, X.; Wang, G. An electrochemical sensor on the hierarchically porous Cu-BTC MOF platform for glyphosate determination. *Sens. Actuators, B* **2019**, *283*, 487−494.
(29) Azizi, A.; Feijani, E. A.; Ghorbani, Z.; Tavasoli, A. Fabrication and characterization of highly efficient three component CuBTC/graphene oxide/PSF membrane for gas separation application. *Int. J. Hydrogen Energy* **2021**, *46*, 2244−2254.
(30) Zhao, J.; Zhang, Z.; Yang, S.; Zheng, H.; Li, Y. Facile synthesis of MoS2 nanosheet-silver nanoparticles composite for surface enhanced Raman scattering and electrochemical activity. *J. Alloys Compd.* **2013**, *559*, 87−91.
(31) Liu, S.; Zhang, X.; Shao, H.; Xu, J.; Chen, F.; Feng, Y. Preparation of MoS2 nanofibers by electrospinning. *Mater. Lett.* **2012**, *73*, 223−225.
(32) Wang, Y.-H.; Huang, K.-J.; Wu, X. Recent advances in transition-metal dichalcogenides based electrochemical biosensors: A review. *Biosens. Bioelectron.* **2017**, *97*, 305−316.
(33) Pakchin, P. S.; Ghanbari, H.; Saber, R.; Omidi, Y. Electrochemical immunosensor based on chitosan-gold nanoparticle/carbon nanotube as a platform and lactate oxidase as a label for detection of CA125 oncomarker. *Biosens. Bioelectron.* **2018**, *122*, 68−74.
(34) Johari-Ahar, M.; Rashidi, M. R.; Barar, J.; Aghaie, M.; Mohammadnejad, D.; Ramazani, A.; Karami, P.; Coukos, G.; Omidi, Y. An ultra-sensitive impedimetric immunosensor for detection of the serum oncomarker CA125 in ovarian cancer patients. *Nanoscale* **2015**, *7*, 3768−3779.
(35) Wu, L.; Sha, Y.; Li, W.; Wang, S.; Guo, Z.; Zhou, J.; Su, X.; Jiang, X. One-step preparation of disposable multi-functionalized g-C3N4 based electrochemiluminescence immunosensor for the detection of CA125. *Sens. Actuators, B* **2016**, *226*, 62−68.
(36) Pakchin, P. S.; Fathi, M.; Ghanbari, H.; Saber, R.; Omidi, Y. A novel electrochemical immunosensor for ultrasensitive detection of CA125 in ovarian cancer. *Biosens. Bioelectron.* **2020**, *153*, 112029.
(37) Gasparotto, G.; Costa, J. P. C.; Costa, P. I.; Zaghete, M. A.; Mazon, T. Electrochemical immunosensor based on ZnO nanorods-Au nanoparticles nanohybrids for ovarian cancer antigen CA125 detection. *Mater. Sci. Eng., C* **2017**, *76*, 1240−1247.
(38) Taleat, Z.; Ravalli, A.; Mazloum-Ardakani, M.; Marrazza, G. CA 125 Immunosensor Based on Poly-Anthranilic Acid Modified Screen-Printed Electrodes. *Electroanalysis* **2013**, *25*, 269−277.

https://doi.org/10.1021/acsabm.1c00324
ACS Appl. Bio Mater. 2021, 4, 5494−5502